

Formation of Fe₃Pt phase in FePt-based nanocomposite magnets

Chuan-bing Rong¹, Vikas Nandwana¹, Narayan Poudyal¹,
Yang Li¹, J Ping Liu¹, Yong Ding² and Zhong Lin Wang²

¹ Department of Physics, The University of Texas at Arlington, Arlington, TX 76019, USA

² School of Materials Science and Engineering, Georgia Institute of Technology, Atlanta, GA 30332, USA

E-mail: pliu@uta.edu

Received 13 September 2006, in final form 17 November 2006

Published 19 January 2007

Online at stacks.iop.org/JPhysD/40/712

Abstract

Atomic interdiffusion between FePt and Fe₃O₄ nanoparticles in annealed FePt-based nanocomposite magnets has been studied by means of structural and magnetic characterizations. The results show that the Fe₃Pt phase is formed during the annealing only when the mass ratio x of Fe₃O₄/FePt is larger than 1/20. When $x \leq 1/20$, only FePt single phase is formed. It is interesting to find that the coercivity of the annealed samples increases with a small addition of Fe₃O₄ before the formation of the Fe₃Pt phase. This magnetic hardening behaviour indicates that the composition of the FePt phase can be further adjusted via the post annealing process. The characteristic of recoil loops and Henkel plots also give evidence for the transition from single-phase FePt magnets to nanocomposite magnets with the addition of Fe₃O₄.

(Some figures in this article are in colour only in the electronic version)

1. Introduction

The $L1_0$ -type FePt nanoparticles have attracted great attention because of their potential applications in ultrahigh-density magnetic recording [1] and advanced permanent magnets [2, 3]. Extensive studies on the chemical synthesis and postannealing of FePt nanoparticle systems have been reported during the past several years [4–9]. It is well known that as-synthesized FePt nanoparticles take a disordered face-centred cubic (fcc) structure which has low magnetocrystalline anisotropy. To develop the $L1_0$ FePt phase with high uniaxial magnetocrystalline anisotropy, heat treatment is necessary to convert the fcc structure to the ordered face-centred tetragonal (fct) structure. Recently, Zeng *et al* [2] fabricated the FePt–Fe₃O₄ nanoparticle self-assemblies by chemical synthesis and obtained the high energy product $(BH)_{\max}$ of 20.1 MGOe. They found that the postannealing, which is necessary for the transition from the fcc to the fct phase, leads to the formation of the Fe₃Pt phase in the FePt-based nanocomposite. This phenomenon is also observed in Fe–Pt thin films [10] and bulk samples [11, 12]. The formation of the Fe₃Pt phase indicates the atomic interdiffusion in FePt-based magnets,

which prevents the formation of FePt–Fe nanocomposite that may have higher $(BH)_{\max}$. In this work, we study the atomic interdiffusion between Fe₃O₄ and FePt and the formation of the Fe₃Pt phase in the FePt-based nanocomposite magnets by crystalline structural and magnetic characterizations. The results show that the Fe₃Pt phase can be obtained only when the Fe₃O₄/FePt mass ratio is high enough. Addition of Fe₃O₄ to some extent leads to an increase in coercivity, which is further evidence of the atomic interdiffusion in the FePt-based nanocrystalline magnets.

2. Experimental details

The high-temperature decomposition of Fe(CO)₅ and reduction of Pt(acac)₂ in solution were used to produce monodisperse 4 nm FePt nanoparticles [13]. The synthesis of 10 nm Fe₃O₄ nanoparticles was carried out using standard airless procedures and commercially available reagents, which were introduced in detail by Sun *et al* [14]. The FePt and Fe₃O₄ nanoparticles were mixed with different mass ratios before centrifugation. Then the mixture was deposited on a Si substrate and annealed under forming gas (Ar+7%H₂) at

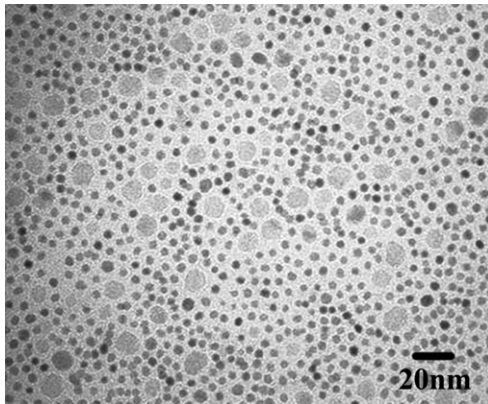


Figure 1. TEM micrographs of self-assembly $\text{Fe}_3\text{O}_4/\text{FePt}$ nanoparticles with $x = 1/8$.

923 K for 1 h. The assembly of nanoparticles was checked by transmission electron microscopy (TEM). The composition of the synthesized FePt nanoparticles is determined by energy dispersive x-ray (EDX) analysis. The crystalline structure was determined by x-ray diffraction (XRD). The room temperature magnetic properties were studied by a superconducting quantum interference device (SQUID) magnetometer with a maximum applied field of 7 T. The field was applied along the longitudinal direction of the annealed films so the demagnetization factor can be neglected. Thermomagnetic curves were measured by a physical properties measurement system (PPMS) with a high-temperature vibrating sample magnetometer.

3. Results and discussions

Figure 1 shows the typical TEM images of mixed Fe_3O_4 –FePt nanoparticles with mass ratio $x = 1/8$. The darker particles are 4 nm FePt and the lighter particles are 10 nm Fe_3O_4 . The contrast between the two kinds of particles is due to the different electron penetration efficiency on metallic FePt and oxide Fe_3O_4 . EDX analysis shows that the composition of synthesized FePt nanoparticles is about $\text{Fe}_{45}\text{Pt}_{55}$. As shown in figure 1, each Fe_3O_4 particle is separated and surrounded by the FePt particles. This assembly structure is similar to that reported previously [2].

Figure 2 shows the XRD patterns of the as-synthesized assembly with $x = 1/5$ and the annealed samples with different x . The grain size of the as-synthesized FePt nanoparticles, which is determined by the Scherrer formula, is around 4.4 nm. This agrees with the TEM analysis. As presented in the previous works, thermal annealing under forming gas will lead to a transformation from the FePt– Fe_3O_4 system to the $L1_0$ FePt– Fe_3Pt system. Our XRD patterns confirmed the transition of the main phase from disordered fcc structure to ordered fct structure. It is interesting to find that the intensity ratio of (220) to (202) peaks increases with increasing x . Because of the absence of a (202) peak for the Fe_3Pt phase, the variation of the intensity ratio should be due to the increase of Fe_3Pt phase content with increasing x . The quantitative analysis of the lattice parameters and the phase content can be made approximately by using the method of the Rietveld refinement on XRD patterns [15]. As an example, the

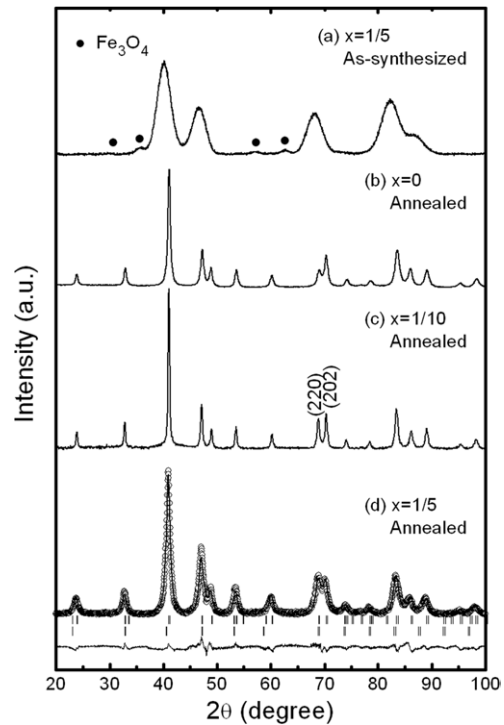


Figure 2. XRD patterns of (a) the as-synthesized assembly with $x = 1/5$ and the annealed samples with different (b) $x = 0$, (c) $1/10$ and (d) $1/5$. The Rietveld refinement data are also included in (d) as well as the observed (O) and calculated (full line) XRD profiles of the annealed sample with $x = 1/5$. The vertical bars represent the Bragg reflection positions of the observed phases (from top to bottom: fct FePt and Fe_3Pt). The difference curve is plotted at the bottom.

Rietveld refinement data of the annealed sample with $x = 1/5$ is also shown in figure 2(d).

Figure 3(a) gives the dependence of lattice parameters (a , c) on x . It shows that the lattice parameters of the FePt single-phase ($a = 3.867 \text{ \AA}$, $c = 3.740 \text{ \AA}$) are larger than those of the standard FePt phase with 50 : 50 Fe : Pt ratio ($a = 3.85 \text{ \AA}$, $c = 3.71 \text{ \AA}$) [16]. This is not surprising since the Fe : Pt atomic ratio in the original FePt phase in this work is about 45 : 55. The extra Pt must substitutionally occupy the Fe sublattice, which will make the unit cell bigger. With the addition of Fe_3O_4 , the parameter c decreases rapidly when $x < 1/20$. This behaviour should be due to the Fe atomic diffusion from Fe_3O_4 to FePt and thus the tendency of the formation of the FePt phase with 50 : 50 Fe : Pt ratio. More addition of Fe_3O_4 would lead to the formation of the two-phase FePt– Fe_3Pt nanocomposite and thus the lattice parameters of $L1_0$ FePt phase change little. Figure 3(b) gives the dependence of volume fraction of Fe_3Pt (v_s) on x . It is found that v_s basically stays at zero for $x \leq 1/20$ since Fe atoms in Fe_3O_4 nanoparticles are mostly diffused into the FePt phase, which agrees with the lattice parameter analysis shown in figure 3(a). When $1/20 < x \leq 1/7$, v_s increases significantly with x , and the increasing tendency of v_s becomes slow when $x > 1/7$. We attribute this behaviour to the further Fe atomic diffusion to the FePt phase under higher Fe_3O_4 content. Figure 3(b) also presents the dependence of average grain size on x . It shows that the diffusion between FePt and Fe_3O_4 led to an increase in

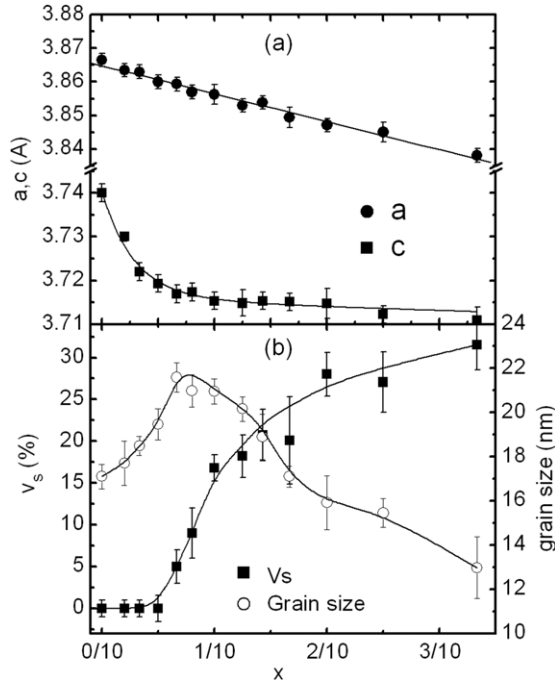


Figure 3. The dependence of (a) a , c and (b) v_s and average grain size on x . The lines are guides to the eye.

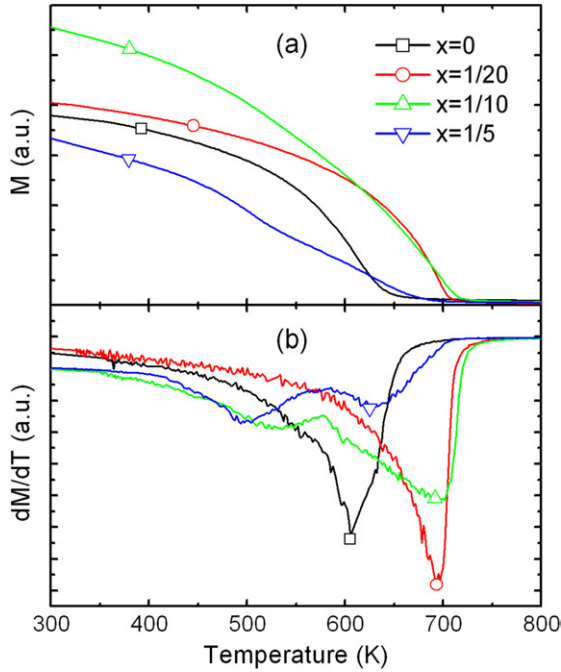


Figure 4. Temperature dependence of (a) magnetization M and (b) dM/dT of the annealed samples with different x .

the grain size when $x \leq 1/15$, while a large amount of Fe_3O_4 led to separated FePt grains and thus decreased grain size.

Figure 4 gives the temperature dependence of magnetization M and dM/dT of the annealed $\text{Fe}_3\text{O}_4/\text{FePt}$ samples with different x . There is only one inflection in the $M-T$ scans and one peak in the $dM/dT-T$ curves of the samples with $x \leq 1/20$ at high temperature. It implies that the annealed samples with low x are almost of a single FePt phase, which is consistent

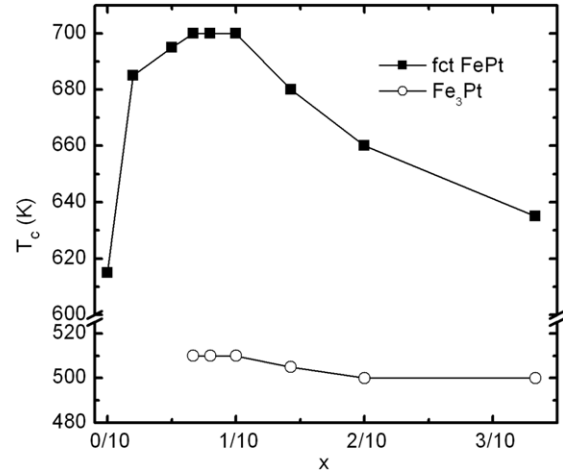


Figure 5. The dependence of T_c^h and T_c^s on x .

with the above refinement results. Two points of inflection occur in the $M-T$ scans for samples with $x \geq 1/15$. The low- and high-temperature inflection points correspond to the Curie temperatures of soft phase Fe_3Pt (T_c^s) and hard phase $L1_0$ FePt (T_c^h). The existence of the two phases is also confirmed by the peaks of the $dM/dT-T$ curves. It is worth noting that the compositions of the FePt phase have a broad distribution as shown by a slow drop of magnetization above the temperature T_c^s . Figure 5 presents T_c^h and T_c^s determined by the maximum of dM/dT . It shows clearly that T_c^h increases with a small Fe_3O_4 addition. Since the variation of T_c^h is an indicator of the Fe:Pt ratio in the FePt phase [17], the fast increase in T_c^h indicates the atomic interdiffusion between FePt and Fe_3O_4 during the annealing. Then T_c^h reached the maximum value of about 700 K for $x = 1/15-1/10$. Simultaneously, T_c^s was almost stable at about 500–510 K for $x \geq 1/15$. The stable T_c^s and T_c^h in this region are caused by the fast increase in v_s since the extra addition of the Fe_3O_4 phase has been transferred to the Fe_3Pt phase instead of diffusion into the $L1_0$ FePt phase as discussed in figure 3. Finally, T_c^h began to decrease with more addition of Fe_3O_4 since more Fe atoms were forced to diffuse into the $L1_0$ FePt phase.

Figure 6 shows the dependence of saturation magnetization M_s and coercivity H_c on x . Since M_s of the $L1_0$ phase increases with Fe:Pt atomic ratio and is lower than that of Fe_3Pt soft-phase, M_s of the annealed samples increases monotonously with x , no matter where the Fe atoms of Fe_3O_4 exist. However, it is interesting to find that H_c increases on raising x for $x \leq 1/15$. Then H_c begins to decrease with a further addition of Fe_3O_4 . With the required high M_s and H_c , the highest energy product $(BH)_{\max}$ of about 17 MGOe can be obtained in the sample with $x = 1/5$. The enhancement of coercivity with Fe_3O_4 addition can be explained in the following discussion. It was reported that the magnetic anisotropy constant K_u of $\text{Fe}_y\text{Pt}_{100-y}$ alloy is sensitive to the composition. For example, K_u is only 0.7×10^7 erg cm^{-3} for $y = 45$ [18] while it is as high as 6.6×10^7 erg cm^{-3} for the stoichiometric composition of $y = 50$ [19]. Since y is about 45 for the original FePt phase in this work, H_c is only 6.5 kOe for the annealed films without Fe_3O_4 . As the atomic interdiffusion between Fe_3O_4 and FePt nanoparticles was extensive

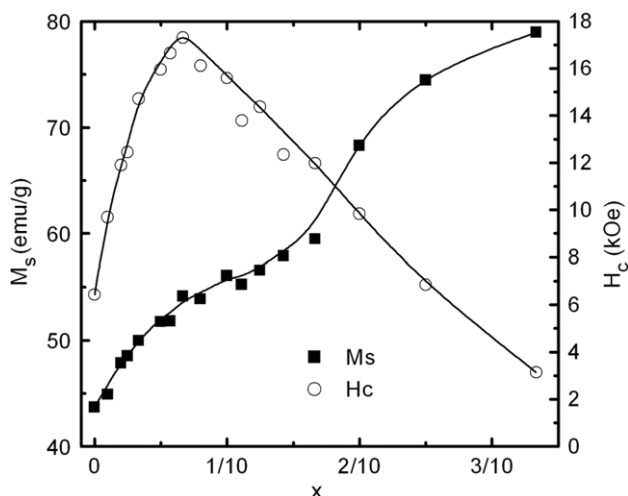


Figure 6. The dependence of M_s and H_c on x .

during annealing under forming gas, the annealed sample was still single-phase until $x \geq 1/15$. Thus, the addition of Fe_3O_4 will lead to an increase in the Fe : Pt ratio in the $L1_0$ phase and reach the optimal Fe composition for the maximum H_c of about 17.5 kOe at $x = 1/15$. It should be noted that the chemical ordering parameter S is almost fixed in the range 0.75–0.80 with varying x . The definition of S has been given in [10]. Thus, the increase in H_c with the addition of Fe_3O_4 is mainly caused by the enhanced magnetic anisotropy with increasing Fe : Pt ratio of FePt alloy. This is different from that reported in [12] in which H_c decreasing with increasing Fe content was found to be due to the decreased S . On the other hand, H_c should decrease if there is no atomic interdiffusion since the soft phase often leads to a decrease in H_c for nanocomposite magnets. Therefore, the enhancement of H_c with the addition of Fe_3O_4 , to some extent, is an indirect evidence of the atomic interdiffusion between Fe_3O_4 and FePt. Further addition of Fe_3O_4 results in the formation of a large amount of Fe_3Pt soft-phase and thus leads to the decrease in H_c .

As discussed above, there exists a transition from single-phase to two-phase with increasing x due to Fe atomic diffusion. Several magnetization behaviours can be used to distinguish the exchange-coupled nanocomposites from single-phase nanocrystalline magnets, such as the recoil loops and Henkel plots. Figures 7(a) and (b) present the recoil loops of the samples with $x = 1/20$ and $1/5$, respectively. The recoil loops are almost close and relatively flat for the $x = 1/20$ sample, which means that it mainly consists of a single phase. This conclusion agrees with the phase structure and thermomagnetic analyses. On the other hand, the recoil loops of the $x = 1/5$ sample are open and steep, which implies a two-phase microstructure in the annealed sample [20–24]. This means that the content of Fe_3O_4 is high enough for the formation of soft phase after the atomic interdiffusion between FePt and Fe_3O_4 .

The usual way to monitor the intergrain magnetic interactions is by constructing the δm plot (Henkel plot) [25–29]. For nanocrystalline single-phase magnets, $\delta m(H)$ always has high positive values, indicating an exchange type of interactions. These interactions suddenly drop to zero or small negative values during reversal as a result of

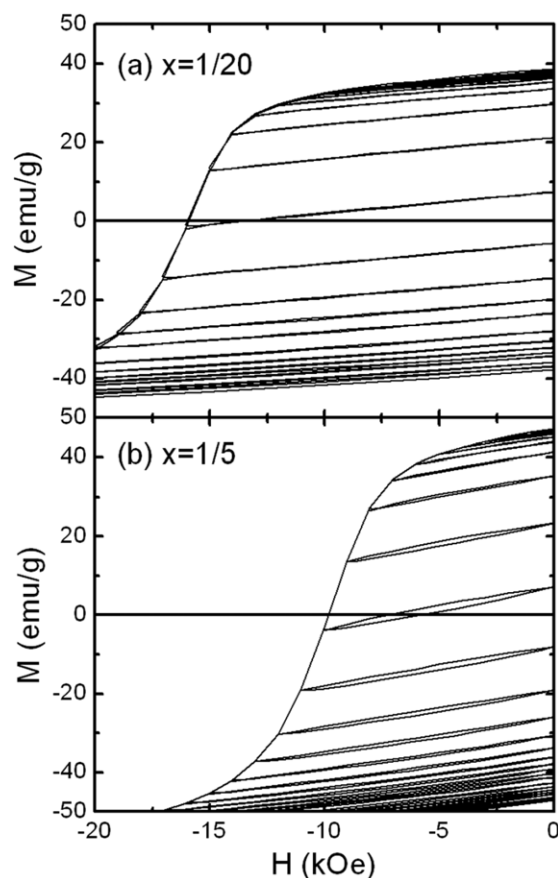


Figure 7. Recoil curves of the samples with (a) $x = 1/20$ and (b) $1/5$.

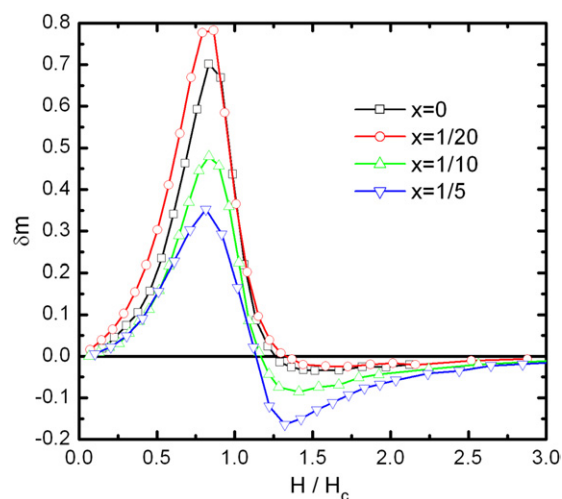


Figure 8. δm plots of the samples with different x .

the cooperative switching of the exchange-coupled grains. In the composite samples $\delta m(H)$ is initially positive also due to the existence of the hard phase that prevents the demagnetization of the sample, but the maximum δm value is always lower than that of single-phase. More important behaviour is that $\delta m(H)$ becomes large negative after the reversal, indicating that magnetostatic interactions become dominant due to the low anisotropy of soft-phase. Figure 8

shows the δm plots of the sample with different x . As can be seen, the exchange coupling in the single-phase magnet with $x = 0$ is very strong even when the coercivity is low. The small addition of Fe_3O_4 caused the enhancement of δm and the exchange coupling, which means that the sample still consists of the FePt single-phase. With the further increase in x , the positive part of $\delta m(H)$ decreases gradually and the negative part becomes more pronounced, showing that the importance of magnetostatic interactions increases with the soft phase content. The influence of the soft-phase content on the behaviour of δm plots is very similar to that of ball-milling PrFeB/ α -Fe nanocomposites [28]. The effect of magnetostatic interactions on the magnetization behaviours of the hard/soft nanocomposite magnets has been reported by our recent works using a micromagnetic model [30].

4. Conclusion

The effects of the $\text{Fe}_3\text{O}_4/\text{FePt}$ mass ratio x on the crystalline structure, magnetic properties and magnetization behaviours have been studied systematically for annealed nanocrystalline magnets. Phase structure and thermomagnetic analysis show that the two-phase FePt– Fe_3Pt nanocomposite can be obtained only with $x > 1/20$, while the annealed films only consist of the FePt single-phase as $x \leq 1/20$ due to the atomic diffusion between FePt and Fe_3O_4 during the annealing. The Fe atomic diffusion also leads to the interesting coercivity behaviour that H_c of the annealed films increases with a small addition of Fe_3O_4 . The characteristic of recoil loops and δm plots prove the transition from single-phase FePt to nanocomposite magnets with the addition of Fe_3O_4 .

Acknowledgments

This work was supported by the US DoD/MURI grant N00014-05-1-0497 and the DARPA through the ARO under Grant No DAAD 19-03-1-0038.

References

- [1] Weller D, Moser A, Folks L, Best M E, Lee W, Toney M F, Schwickert M, Thiele J U and Doerner M F 2000 *IEEE Trans. Magn.* **36** 10
- [2] Zeng H, Li J, Liu J P, Wang Z L and Sun S H 2002 *Nature* **420** 395
- [3] Rong C B, Zhang H W, Chen R J, He S L and Shen B G 2006 *J. Magn. Magn. Mater.* **302** 126
- [4] Yu A C C, Mizuno M, Sasaki Y, Kondo H and Hiraga K 2002 *Appl. Phys. Lett.* **81** 3768
- [5] Shevchenko E V, Talapin D V, Rogach A L, Kornowski A, Haase M and Weller H 2002 *J. Am. Chem. Soc.* **124** 11480
- [6] Kang S S, Harrell J W and Nikles D E 2002 *Nano Lett.* **2** 1033
- [7] Chen M, Liu J P and Sun S H 2004 *J. Am. Chem. Soc.* **126** 8394
- [8] Zeng H, Sun S H, Li J, Wang Z L and Liu J P 2004 *Appl. Phys. Lett.* **85** 792
- [9] Liu J P, Luo C P, Liu Y and Sellmyer D J 1998 *Appl. Phys. Lett.* **72** 483
- [10] Rong C B, Li D R, Nandwana V, Poudyal N, Ding Y, Wang Z L, Zeng H and Liu J P 2006 *Adv. Mater.* **18** 2984
- [11] Hai N H, Dempsey N M and Givord D 2003 *J. Magn. Magn. Mater.* **262** 353
- [12] Lyubina J, Gutfleisch O, Müller K H and Schultz L 2005 *J. Magn. Magn. Mater.* **290–291** 547
- [13] Sun S H, Murray C B, Weller D, Folks L and Moser A 2000 *Science* **287** 1989
- [14] Sun S H, Zeng H, Robinson D B, Raoux S, Rice P M, Wang S X and Li G X 2004 *J. Am. Chem. Soc.* **126** 273
- [15] Lyubina J, Opahle I, Muller K H, Gutfleisch O, Richter M, Wolf M and Schultz L 2005 *J. Phys.: Condens. Matter* **17** 4157
- [16] JCPDS-International Centre for Diffraction Data 1999 Card no 43-1359
- [17] Barmak K, Kim J, Berry D C, Hanani W N, Wierman K, Svedberg E B and Howard J K 2005 *J. Appl. Phys.* **97** 24902
- [18] Wu X W, Guslienko K Y, Chantrell R W and Weller D 2003 *Appl. Phys. Lett.* **82** 3475
- [19] Vlasova N I, Kandaurova G S and Shchegoleva N N 2000 *J. Magn. Magn. Mater.* **222** 138
- [20] Panagiotopoulos I, Withanawasam L and Hadjipanayis G C 1996 *J. Magn. Magn. Mater.* **152** 353
- [21] Feutrell E H, McCormick P G and Street R 1996 *J. Phys. D: Appl. Phys.* **29** 2320
- [22] Goll D, Seeger M and Kronmuller H 1998 *J. Magn. Magn. Mater.* **185** 49
- [23] Zhang H W, Zhao T Y, Rong C B, Zhang S Y, Han B S and Shen B G 2003 *J. Magn. Magn. Mater.* **267** 224
- [24] Harland C L, Lewis L H, Chen Z and Ma B M 2004 *J. Magn. Magn. Mater.* **271** 53
- [25] Wohlfarth E P 1958 *J. Appl. Phys.* **29** 595
- [26] O'Grady K, El-Hilo M and Chantrell R W 1993 *IEEE Trans. Magn.* **29** 2608
- [27] Zhang H W, Rong C B, Zhang J, Zhang S Y and Shen B G 2002 *Phys. Rev. B* **66** 184436
- [28] Bollero A, Gutfleisch O, Muller K-H, Schultz L and Drazic G 2002 *J. Appl. Phys.* **91** 8159
- [29] Rong C B, Zhang H W, Shen B G and Liu J P 2006 *Appl. Phys. Lett.* **88** 42504
- [30] Rong C B, Zhang H W, Chen R J, He S L and Shen B G 2006 *J. Magn. Magn. Mater.* **302** 126